Flow Turbulence Combust (2015) 95:803–829
DOI 10.1007/s10494-015-9642-0

Diffusion MILD Combustion of Firing Pulverized-coal at a Pilot Furnace

Z. Mei[1,2] · P. Li[1] · J. Mi[1,3] · F. Wang[4] · J. Zhang[1]

Received: 5 October 2014 / Accepted: 28 April 2015 / Published online: 1 September 2015

Abstract This paper presents the computational investigation of the diffusion MILD (Moderate or Intense Low-oxygen Dilution) combustion of firing pulverized-coal at a pilot furnace. Dependences of the combustion performance are examined on the injection parameters, e.g., the fuel injection angle and the separation between the primary and secondary nozzles. Calculations are performed to examine the combustion characteristics, e.g., velocity and temperature distributions, CO and NO emissions, and char burnout. The validation of the modeling is carried out using the experimental measurements of Weber et al. (Proc. Combust. Inst. **30**, 30 (2), 2623–2629 2005). Results reveal that an increase in the fuel injection angle or the separation reduces the peak temperature in the confluence region of the primary and secondary streams and thus the exhaust NO emission. During the coal MILD combustion, the (destroying) NO reburning mechanism is strongly involved so that the NO emission is below the NO production from the fuel-NO route, given that other routes of NO formation are unimportant. It is also found that the gasification reactions of char with CO_2 and H_2O in coal MILD combustion appear to compensate for depression of the low O_2 concentration on the coal burnout. In addition, several suggestions are made that could be useful for design of coal MILD burners.

✉ J. Mi
jmi@pku.edu.cn

[1] Department of Energy & Resources Engineering, College of Engineering, Peking University, Beijing 100871, People's Republic of China

[2] National Engineering Research Center for Clean Coal Combustion, Xi'an Thermal Power Research Institute, Xi'an, 710054, China

[3] College of Energy & Power Engineering, Changsha University of Science and Technology, Changsha, 410004, China

[4] Department of Building Environment & Equipment Engineering, School of Environmental Science & Engineering, Huazhong University of Science & Technology, Wuhan, 430074, China

Keywords MILD combustion · Pulverized-coal · Injection angle · NO_x emission

1 Introduction

Since early 1990, MILD combustion has continuously gained attention from the combustion community and also the industry sector, primarily because it can achieve both high efficiency and low NOx emissions simultaneously [1–30]. This combustion may be characterized as follows: both fuel and oxidizer are deeply diluted by the flue gas recirculated, so that their chemical reactions occur slowly and thus heat release takes place over a volume much larger than for conventional combustion. Consequently, the peak temperature drops significantly, resulting in a great reduction of NO_x formation. The MILD combustion is sometimes termed also as "Flameless Oxidation (FLOX)" or "Flameless Combustion (FC)", from a descriptive form of the resulting combustion process, and "High Temperature Air Combustion (HiTAC)" according to the features of reactant streams. Of note, the MILD combustion technologies were developed nearly simultaneously by Wünning & Wünning in Germany [1, 2], the International Flame Research Foundation (IFRF) [3, 4] and Nippon Furnace Kogyo Kaisha Ltd. (NFK-Japan) [5, 6] in 1990's. It follows that, over last 2.5 decades or so, this combustion has been extensively investigated in the combustion community, especially, by Blasiak's group [7, 8], Cavaliere's group [9, 10], Costa's group [11, 12], Dally's group [13, 14], Gupta's group [15, 16], Kumar's group [17, 18], Mi's group [19–25], Rota's group [26, 27] and Weber's group [28, 29], among others.

A large amount of research on MILD combustion, either by experiment or numerical simulation, has been conducted for NG (natural gas) [13, 14, 19–23, 31, 32] and LPG (liquefied petroleum gas) [7, 21, 31, 33]. It has been found that both the establishment and performance of the combustion depend on the operating parameters, e.g., equivalence ratio [19, 20, 31], fuel dilution [13, 19, 31], oxygen concentration [14, 21, 23], oxidizer/fuel injection velocity [19, 21–23], fuel temperature [7, 19, 23], air preheated temperature [19, 23, 32], separation distance of fuel-air nozzles [19, 23] and fuel injection angle [19]. By optimizing the operating parameters for MILD combustion, both low temperature peaks (e.g., 1200 K) [21] and suppressed NO_x emissions (e.g., 15 ppm at 3 % O_2) [14] were obtained.

So far, several experimental studies have confirmed that MILD combustion can also apply for pulverized coal and similar advantages may be achieved [29, 34–39]. However, the MILD combustion of pulverized coal is somehow distinct from that of gaseous fuels which is flameless or has no visible flame at all [2, 6, 30]. For the former, the true "flameless" combustion has never been observed and there are always discernible sparks existing [24, 29, 34]. That is, although the volatile gas is burning perhaps invisibly, the char particles are just firing under the MILD condition and the relatively long firing time of char particles [40] leads to visible sparks. Moreover, the source of nitric oxide (NO_x) of MILD combustion of pulverized coal differs significantly from that of gaseous fuels. The NO_x formation (and then emissions) of pulverized-coal combustion results from the oxidations of both fuel-N in coal and N_2 in air while that of gaseous fuel derives primarily from the latter. Consequently, previous observations and conclusions obtained from the MILD combustion of firing gaseous fuels may not entirely apply for the case of firing pulverized coal. It follows that the effects of operating parameters on the temperature distribution and NO_x emissions should be investigated for the latter case.

Table 1 summarizes several previous experiments and simulations [24, 25, 35–39, 41–43]. Suda et al. [35] experimentally investigated the effects of the inlet air temperature (623 and 1073 K) on ignition, burnout and NO_x emission for the high-volatile bituminous

Table 1 Previous parametric studies on MILD combustion of pulverized coal

Year	Ref.	Method	Capacity	Volatile & N element in coal (mass fraction)	Operating parameters
2002	Suda et al. [35]	Exp.	250 kW	9.8∼43.9 % & 0.9∼1.3 %	Air temperature (623∼1073 K)
2007	Zhang et al. [36]	Exp.	12 MW	7.8∼11.6 % & 1.78∼3.39 %	PRP (primary air enrichment and preheating) burner vs conventional LNB (low NOx burner)
2008	Ponzio et al.[37]	Exp.	N/A	19.4 % & 1.5 %	O_2 concentration (5∼100 vol %) Oxidizer temperature (873∼1273 K)
2009	Rathnam et al. [38]	Exp.	N/A	24.5∼40.5 % & 1.16∼2.14 %	O_2 (3∼21 vol %)/N_2 O_2 (5∼30 vol %) /CO_2
2009	Stadler et al. [39]	Exp.	5∼8 kW, 40 kW	21.6∼48.7 % & 0.55∼1.41 %	Air, O_2/Ar and O_2/CO_2 MILD vs flame mode Excess air ratio (0.7∼1.0) O_2 (15∼25 vol %)
2009	Stadler et al. [41]	CFD	40 kW	33 % & 1.41 %	Wall temperature (900∼1500 K) Excess air ratio (0.7∼0.9)
2010	Mancini et al. [42]	CFD	130 MW	37.1 % & 1.5 %	Boiler shape and dimensions Burner configuration (a boiler with 1∼5 burners) and location (down-fired and up-fired) Air excess ratio (1.05∼1.2) Air temperature (300∼900 K) Secondary air velocity (60∼120 m/s)
2011	Shaddix et al. [43]	Exp.	N/A	3.3∼40.4 % & 0.9∼1.6 %	O_2 (12∼36 vol %) O_2/N_2 and O_2/CO_2
2014	Mei et al. [25]	CFD	0.58 MW	37.1 % & 1.5 %	Primary air velocity (26∼ 99 m/s) Secondary air velocity (16∼ 102 m/s)
2014	Li et al. [24]	Exp.	0.3 MW	18.74 % & 1.45 %	Conventional air combustion MILD air combustion MILD oxy-combustion

coal. They observed that the measured peak temperature and NO_x emission were lower by about 100 K and 155 ppm (dry at 6 % O_2), respectively, in the 1073 K case. Stadler et al. [39] conducted experiments investigating the NO_x emissions from coal MILD combustion in air, O_2/Ar and O_2/CO_2 conditions. These investigators found that, for the coal combustion in air, the total NO emissions at the furnace exit was about 25 % lower in the MILD mode than in the conventional flame mode. Based on the different NO emissions for the O_2/N_2 and O_2/Ar conditions, they estimated that the thermal NO from the MILD combustion was only about half of that from the conventional combustion. Later, the same research group [41] numerically investigated the effects of the wall temperature and the burner excess air ratio on the NO formation in coal MILD combustion. The lowest NO emission (110 ppm) was achieved with the wall temperature = 1673 K and the burner excess ratio = 0.7. They suggested that efforts in the burner design for coal MILD combustion should be made to promote the intense mixing between recirculated hot combustion products and incoming fresh reactants, thus achieving simultaneous fast O_2 dilution and fuel heat-up. Mancini et al. [42] numerically investigated the effects of boiler shape and dimensions, burner configuration and location on the MILD combustion in the supercritical pulverized coal boiler (130 MW). Based on the simulations, they designed an optimal conceptual configuration of the burner and boiler and examined the impact of the air excess ratio, the preheated temperature and injection velocity of the air. The momentum of the combustion air stream was found to be an essential design parameter driving the in-furnace recirculation whereas the impact of the combustion air temperature on boiler performance is less critical, providing that the intensive in-furnace recirculation has been created. Shaddix et al. [43] experimentally investigated the effects of oxygen concentrations (at the air temperature of 1320 K) on the NO_x formation during the combustion of pulverized coals. They found that when the O_2 concentration is varied from 12 to 36 vol %, the fractional fuel-N conversion to NO_x increased dramatically from 20 to 50 % for a typical US high-volatile bituminous coal and from 40 to 90 % for a typical US subbituminous coal. They also found that the fuel-N conversion fractions are slightly lower in O_2/CO_2 condition relative to O_2/N_2 condition. Very recently, we numerically investigated the effects of reactant injection velocities on coal MILD combustion [25] in the IFRF (International Flame Research Foundation) furnace [29]. The simulation indicated that increasing the primary air velocity has strong effects on reducing the temperature peak (by about 180 K) and NO_x emissions (by about 200 ppm), while increasing the secondary air velocity has weak effects on reducing the temperature peak (<50 K) and the NO emission (<10 ppm). We also experimentally investigated the MILD air combustion and oxy-combustion in a pilot-scale furnace [24]. The MILD combustion was reached both in air-combustion and oxy-combustion for pulverized coal, and fairly uniform temperature distributions, low NO and CO emissions were obtained. Importantly, the coal MILD combustion was found to reduce the NO emission much more effectively in oxy-combustion than in air combustion. However, all the above experimental and numerical investigations did not cover the effects of the fuel injection angle and the separation distance of the fuel-air nozzles, which are fundamentally important parameters of the burner design, on coal MILD combustion. Our previous studies of firing gaseous fuels [19, 23] have demonstrated that the injection angle and the separation are indeed two key factors affecting temperature distributions and NO emissions. Compared with other parameters, e.g., preheating temperature and injection velocity or momentum, these two parameters were found to be more effective in changing the combustion characteristics. Hence the effects of these two factors on the pulverized-coal combustion should be considered either.

The present study is accordingly proposed to address the above issue by simulating the pulverized-coal combustion in the IFRF furnace, which is a pilot-scale furnace similar to

the practical industrial furnace. The models of devolatilization, gasification, oxidation and turbulence-chemical interaction are adapted to the coal MILD combustion. After the modeling is validated by the measurements of Weber et al. [29], several investigations on the combustion are performed by varying the fuel injection angle (α) between $-10°$ and $+15°$ and the separation distance of the fuel-air nozzles (S) from 0.1 to 0.6 m, with other parameters kept identical with the experiment. The flow fields, char burnouts and temperature distributions in the chamber and the exhaust CO emissions at the furnace exit are examined. The NO emissions of the coal combustion from thermal-NO, prompt-NO, intermediate-N_2O, fuel-NO, and NO-reburning routes are also investigated. Besides, based on the present study and our previous work [25], several suggestions are provided that could be useful for design of coal MILD burners.

2 Computational Description

In the IFRF experiment of the pulverized coal MILD combustion, the measurements were taken by Weber et al. [44] at seven traverse locations over the whole furnace and the furnace exit. Detailed experimental results of the axial velocity, temperature and species (O_2, CO_2, CO and NO_x) provided sufficient references for validations of numerical simulations [44, 45]. With the satisfactory models adopted for the coal MILD combustion, we investigated the effects of the primary and secondary air injection velocities on coal MILD combustion in the IFRF furnace [25]. The modeling details are given below, following a brief description on the experimental setup of IFRF (see Ref. [29] for more details).

2.1 Burner and furnace configurations

The dimensions of the IFRF furnace are 2 m × 2 m × 6.25 m, see Fig. 1. The burner consists of a central pipe (inner diameter = 0.125 m) and two horizontal side pipes (0.0273

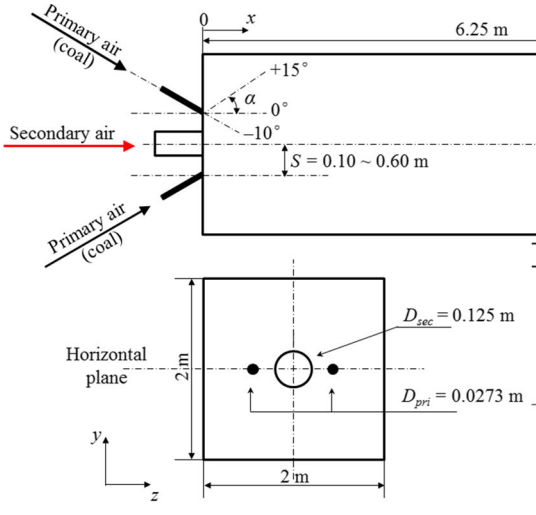

Case	α	S (m)
1	-10°	0.28
2	-5°	0.28
3	0°	0.28
4	+5°	0.28
5	+10°	0.28
6	+15°	0.28
7	0°	0.10
8	0°	0.15
9	0°	0.28
10	0°	0.45
11	0°	0.60

Fig. 1 Configurations of the present burner and the IFRF furnace

m) which are located 0.28 m away from the burner center. A highly volatile bituminous coal with 1.5 % N (dry and ash-free basis) is combusted. The ultimate and proximate analyses of the coal are given in Table 2. The primary air carrying the pulverized coal is injected into the furnace via the two side pipes, while the secondary air enters the furnace from the central pipe. In the experiment of Weber et al. [29], the burner was operated at 0.58 MW fuel input and the secondary air was preheated to 1623 K. Under those special inlet conditions of the primary and secondary air (see Table 3), the MILD combustion was successfully achieved for pulverized coal and very low NO emissions were obtained in the flue gases, which is also the lowest NO emissions in the 40-years long IFRF history for the pulverized coal combustion. However, it is uncertain that the burner configuration may be optimized further to obtain lower NO emissions. In the present work, the fuel injection angle (α) varies from $-10°$ to $+15°$, and the separation of the primary-secondary air nozzles (S) varies between 0.1 m and 0.6 m, see Fig. 1.

2.2 Computational models

Due to the symmetry of the furnace system, only one quarter of the geometry is employed to reduce the computational expense, and a 3D grid composed of about 1,190,000 hexahedral cells is used after verifying the grid-independency of the results using a finer grid with 3,500,000 cells. The commercial software FLUENT 6.3 has been used for the present work. The Rosin-Rammler distribution function is adopted to describe the particle size distribution of the coal, and the 10∼300 μm size range is divided into 20 size classes.

Note that the standard $k-\varepsilon$ model and realizable $k-\varepsilon$ model was used by Schaffel et al. [44] and Vascellari et al. [45] for the simulations of the IFRF coal MILD combustion [29], respectively. It is known that the realizable $k-\varepsilon$ model predicts the spreading rate of both planar and round jets more accurately than the standard $k-\varepsilon$ model. The realizable $k-\varepsilon$ model also provides superior performance for flows involving rotation, boundary layers under strong adverse pressure gradients, separation, and recirculation. Thus in the present work, the realizable $k-\varepsilon$ model is employed for the RANS turbulence modeling. It is also believed that the $k-\varepsilon$ model can capture the fluid dynamics in the cases with positive fuel injection angles (α). There are several simulations of high temperature air combustion involving the positive fuel angles in literature. Fleck et al. [46] conducted

Table 2 Characteristics of the Guasare coal

	Composition	wt %		
Proximate analysis	Moisture (105 °C)	2.9		
	Volatile matter	37.1		
	Fixed carbon	56.7		
	Ash	3.3		
	LCV	31.74 (MJ/kg)		
		Coal	Char	Volatiles
Ultimate analysis	C	81.6	92.6	72.51
(dry, ash free basis)	H	5.5	1.3	9.10
	O	10.7	4.0	16.3
	N	1.5	1.7	1.3
	S	0.6	0.4	0.8

Table 3 Experimental condition of Weber et al. [29]

	Mass flow (kg/h)	Velocity (m/s)	Temperature (K)	Enthalpy (MW)	Composition (wt % wet)
Coal	66	–	–	0.58	
Primary air	130	26	313	–	$O_2 = 23$, $N_2 = 77$
Secondary air	675	65	1623	0.30	$O_2 = 22$, $H_2O = 9.5$, $CO_2 = 12.5$, $N_2 = 56$, $NO = 89\times10^{-4}$

experimental and numerical investigation of the low NO_x CGRI (Canadian Gas Research Institute) burner with positive fuel nozzle angles. Turbulence modeling was handled using the $k-\varepsilon$ model. The predicted velocity shows a satisfactory agreement with the LDV (Laser Doppler Velocimetry) measurement. Besides, the $k-\varepsilon$ model was also used by Li et al. [47] and Su et al. [48] to investigate the burners with positive fuel nozzle angles.

In MILD combustion, the chemical reactions take place in a large zone and the reaction rates are comparable to the turbulent mixing rates of reactants [45]. The Eddy Dissipation Model (EDM), which is conventionally used by CFD (computational fluid dynamic) codes for combustion modeling, is based on infinitely fast chemistry assumption and thus cannot correctly reproduce the MILD combustion process. The EDC model, which is an extension of the EDM, has been proved to perform well in describing the slow chemistry of the coal MILD combustion [25]. Then the realizable $k-\varepsilon$ turbulence model [49] and the EDC (Eddy Dissipation Concept) model [50] are taken to consider the interaction between turbulent flow and chemical reaction here. The Discrete Phase Model (DPM) follows the Euler-Lagrange approach. The gaseous phase is treated as a continuum by solving the Navier-Stokes equations, while the dispersed phase (i.e., coal particles) is solved by tracking a large number of particles through the calculated flow field. The dispersed phase can exchange momentum, mass, and energy with the gaseous phase. The dispersion of particles due to turbulence is taken into account by considering the stochastic tracking model (i.e., Discrete Random Walk Model).

The CPD (Chemical Percolation Devolatilization) model [51] is used to characterize the devolatilization behavior of the coal particles in the present simulations. In contrast to the constant rate model, the single kinetic rate model and the two competing rates model (all based on empirical rate relationships), the CPD model characterizes the devolatilization behavior of rapidly heated coal based on the physical and chemical transformations of the coal structure. The CPD parameters, which are adapted to the coal used in the experiment [29], are shown in Table 4. After volatile matter is completely devolatilized, both the oxidation and gasification are considered for the heterogeneous reactions of the char remaining

Table 4 Parameters for the CPD devolatilization model of Guasare coal [44]

Parameter	Value	Unit
Initial fraction of bridges in coal lattice	0.5	–
Initial fraction of char bridges	0	–
Lattice coordination number	5	–
Cluster molecular weight	300	kg/kmol
Side chain molecular weight	30	kg/kmol

in the coal particles: $C_{(s)} + 0.5O_2 \rightarrow CO$, $C_{(s)} + CO_2 \rightarrow 2CO$ and $C_{(s)} + H_2O \rightarrow CO + H_2$. This is because the surrounding gas is usually composed of high CO_2, H_2O and low O_2 in coal MILD combustion. The composition of the volatile is set as $CH_4/CO/H_2$ = 47 %/48 %/5 %. Note that Vascellari et al. [45] demonstrated that the Global Multi-Step Combustion Mechanism (i.e., The Jones and Lindstedt Mechanism [52]) for the volatile is more accurate than the simplified two-step reaction mechanism of the volatile oxidation ($C_{1.2}H_{4.48}O_{0.44} + 1.5O_2 \rightarrow 1.2CO + 2.24H_2O$, $CO + 0.5O_2 \rightarrow CO_2$) used by Schaffel et al. [44] Thus the Jones and Lindstedt Mechanism [52] (i.e., $CH_4 + 0.5O_2 \rightarrow CO + 2H_2$, $CH_4 + H_2O \rightarrow CO + 3H_2$, $H_2 + 0.5O_2 \rightarrow H_2O$ and $CO + H_2O \rightarrow CO_2 + H_2$) is employed to simulate the homogeneous reactions of volatile matter in the gaseous phase here. The P1 radiation model [53] is used for radiation heat transfer and the absorption coefficient of the gas mixtures is assumed to be 1.5 m^{-1}, kept constant through the furnace volume. Solution convergence is obtained when (a) the residuals are less than 10^{-6} for the energy, 10^{-5} for all the other variables and (b) the variations of the outlet temperature and velocity are allowed to be within 1.0 K and 0.1 m/s, respectively.

The post processing approach is conducted to predict the NO emissions. Four distinct chemical kinetic processes (i.e., thermal-NO, prompt-NO, fuel-NO, and intermediate-N_2O) are considered for the formation of NO and the NO-reburning mechanism is considered to predict the reduction of NO. The modeling details can be found in Refs. [44, 45], and only a brief description is provided below.

The thermal-NO is determined by the extended Zeldovich mechanism [54], i.e.

$$O + N_2 \Leftrightarrow N + NO \tag{1}$$

$$N + O_2 \Leftrightarrow O + NO \tag{2}$$

$$N + OH \Leftrightarrow H + NO \tag{3}$$

Then the net rate of NO formation via Reactions (1–3) is calculated by thermal-NO:

$$\frac{d[NO]}{dt} = k_{f,1}[O][N_2] + k_{f,2}[N][O_2] + k_{f,3}[N][OH] - k_{r,1}[N][NO] - k_{r,2}[O][NO] - k_{r,3}[H][NO] \tag{4}$$

The expressions for the rate coefficients $k_{f,1}$ (the rate coefficient for the forward Reaction 1), $k_{f,2}$, $k_{f,3}$, $k_{r,1}$ (the rate coefficient for the backward Reaction 1), $k_{r,2}$ and $k_{r,3}$ are selected based on the evaluation of Hanson and Salimian [55].

It is worth noting that O_2 and N_2 distributions are provided by the previous combustion simulation while the O and OH radicals are not contained in the Kinetic mechanisms. Thus the equilibrium approaches are employed to determine the O and OH radical concentrations, i.e.

$$[O] = 3.97 \times 10^5 T^{-0.5} [O_2]^{0.5} e^{-31090/T} \tag{5}$$

$$[OH] = 2.129 \times 10^2 T^{-0.57} [O]^{0.5} [H_2O]^{0.5} \tag{6}$$

Thus the thermal-NO can be calculated by Eqs. 4–6.

The actual formation of the prompt NO involves a complex series of reactions and many possible intermediate species, and one of the accepted route is given below:

$$CH + N_2 \Leftrightarrow HCN + N \tag{7}$$

$$N + O_2 \Leftrightarrow NO + O \tag{8}$$

$$HCN + OH \Leftrightarrow CN + H_2O \tag{9}$$

$$CN + O_2 \Leftrightarrow NO + CO \tag{10}$$

The rate of the prompt-NO is determined by the De Soete model [56], i.e.

$$\text{prompt NO}: \frac{d[\text{NO}]}{dt} = f \times 6.4 \times 10^6 \times \left(\frac{RT}{p}\right)^{a+1} [\text{O}_2]^a [\text{N}_2][\text{FUEL}] e^{-E_a/RT} \quad (11)$$

where f is a correction factor and depends on the number of carbon atoms per molecule for the hydrocarbon fuel (n) and the equivalence ratio (Φ), R is the universal gas constant, p is pressure, the activation energy $E_a = 303474.125$ J/mol, a is the oxygen reaction order and depends on the local oxygen mole fraction $[\text{O}_2]$. Thus the prompt-NO can be calculated by Eq. 11.

The fuel-NO is originated from the element N in the char and volatiles. The mass fractions of the Char-N and Volatile-N are 1.7 % and 1.3 % (by weight dry, ash free basis), respectively. Similar to Schaffel et al. [44], both the Char-N and Volatile-N are assumed to convert to HCN. This HCN mechanism proposed by Smoot and Smith [57] is described as follows

$$\text{Char-N} \rightarrow \text{HCN}, \quad (12)$$

$$\text{Volatile-N} \rightarrow \text{HCN}. \quad (13)$$

The conversion rates of Char-N and Volatile-N via Reactions 12 and 13 are dominated by the burning rate of char (combustion model: multiple-surface-reactions) and the devolatilization rate of the volatiles from coal particles into gas phase (devolatilization model: CPD), respectively. Then HCN is subject to two competitive reaction paths, i.e.

$$\text{HCN} + \text{O}_2 \rightarrow \text{NO} + \ldots \quad (14)$$

$$\text{HCN} + \text{NO} \rightarrow \text{N}_2 + \ldots \quad (15)$$

The conversion rates of HCN via Reaction 14 (CR_{14}) and 15 (CR_{15}) are proposed by De Soete [56]. Thus the fuel-NO can be calculated by

$$\text{fuel-NO}: \frac{d[\text{NO}]}{dt} = CR_{14} - CR_{15} \quad (16)$$

The intermediate-N_2O path for NO is predicted by Melte and Pratt's mechanism [58], i.e.

$$\text{N}_2 + \text{O} + \text{M} \Leftrightarrow \text{N}_2\text{O} + \text{M} \quad (17)$$

$$\text{N}_2\text{O} + \text{O} \Leftrightarrow 2\text{NO} \quad (18)$$

The O radical concentration [O] is determined by Eq. 5. M is a general third body, and can be determined by

$$[\text{M}] = 1.4[\text{O}_2] + 3.0[\text{CO}_2] + 1.7[\text{N}_2] + 12[\text{H}_2\text{O}] \quad (19)$$

Based on the assumption of quasi-steady-state of N_2O (i.e., $\frac{d[\text{N}_2\text{O}]}{dt} = 0$), $[N_2O]$ can be calculated by

$$k_{f,13}[\text{N}_2][\text{O}][\text{M}] - k_{r,13}[\text{M}][\text{N}_2\text{O}] = k_{f,14}[\text{N}_2\text{O}][\text{O}] - k_{r,14}[\text{NO}]^2 \quad (20)$$

where $k_{f,13}$ and $k_{f,14}$ are the forward rate constants of Reaction 17 and 18, and $k_{r,13}$ and $k_{r,14}$ the corresponding reverse rate constants. Then the NO formation from the intermediate N_2O can be determined by intermediate-N_2O path for NO via:

$$\frac{d[\text{NO}]}{dt} = 2\left(k_{f,14}[\text{N}_2\text{O}][\text{O}] - k_{r,14}[\text{NO}]^2\right) \quad (21)$$

The NO-reburning mechanism in gaseous phase is based on the model proposed by Kandamby et al. [59], i.e.

$$\mathrm{NO} + \mathrm{CH_2} \rightarrow \mathrm{HCN} + \mathrm{OH} \tag{22}$$

$$\mathrm{NO} + \mathrm{CH} \rightarrow \mathrm{HCN} + \mathrm{O} \tag{23}$$

$$\mathrm{NO} + \mathrm{C} \rightarrow \mathrm{CN} + \mathrm{O} \tag{24}$$

The expression of the global NO reduction rate in gas phase is given by NO-reburning with volatile:

$$\frac{d[\mathrm{NO}]}{dt} = -4 \times 10^{-4} \left(5.3 \times 10^{9} T^{-1.54} e^{-\frac{27977}{RT}} + 3.31 \times 10^{13} T^{-3.33} e^{-\frac{15090}{RT}} + 3.06 \times 10^{11} T^{-2.64} e^{-\frac{77077}{RT}}\right) [\mathrm{FUEL}][\mathrm{NO}], \tag{25}$$

where [FUEL] denotes the reburn fuel species concentration which is the sum of the mass fractions of CH_i radicals, including CH_4, CH_3, CH_2 and CH. In the present simulations, CH_3, CH_2 and CH are not involved in the chemical kinetic mechanism. Thus, CH_4 mass fraction is employed for [FUEL].

The NO-reduction on char surface is also considered with the Levy et al.'s model [60], i.e., NO-reduction on char surface:

$$\frac{d[\mathrm{NO}]}{dt} = -2.27 \times 10^{-3} \times [\mathrm{NO}] \times p \times e^{-\frac{142737}{RT}} \times C_s \times A_{BET}. \tag{26}$$

Here C_s is the concentration of particles, and A_{BET} is the pore (BET) surface area.

3 Results and Discussion

3.1 Validation of the modeling

To validate the modeling, the present simulation is performed under the same condition of Weber et al. [14] Fig. 2 compares the predicted distributions of velocity, temperature, CO and NO volume fractions with the measurements at $x = 0.44$, 1.32 and 4.97 m. Note that the secondary air used in the simulations is vitiated with some nitric oxide at 89 ppm (mass fraction) to comply with that of the IFRF experiment [29] (see Table 3). Also, the previous modeling results of Schaffel et al. [44] and Vascellari et al. [45] are included for comparison. Evidently, the present calculated velocities agree well with the measurements except for the centerline velocities at $x = 0.44$ and 1.32 m. Figure 2 also shows that the centerline velocities predicted by Schaffel et al. [44] are closer to the measurements than those predicted by Vascellari et al. [45] and the present simulations. However, from the non-smooth curves of Schaffel et al. [44] at $x = 0.44$ m, it is deduced that their mesh may be not fine in the downstream region around the central nozzle. Besides, they cannot capture the potential core of the central jet at $x = 0.44$ m. Notably, the nozzle diameter of the central jet (D) is 0.125 m and the exit velocity is 65 m/s. The potential core of a round free jet is usually within $0 \leq x/D \leq 5 - 6$, see Ref. [61], and thus the centerline velocity at $x = 0.44$ m $= 3.52D$ should be close to 65 m/s. Unexpectedly, the corresponding predicted value by Schaffel et al. [44] and the measured one [29] is 55 m/s and 47 m/s, respectively. Moreover, even at $x = 0.15$ m (i.e., $x/D = 1.2$) where is quite close to the central nozzle exit, the measured centerline velocity (= 45 m/s) is also significantly lower than 65 m/s. Both Schaffel et al. [44] and Vascellari et al. [45] attributed the distinction to the poor Laser Doppler Anemometer (LDA) measurements [29] at $x = 0.44$ m. Orsino et al. [62] explained

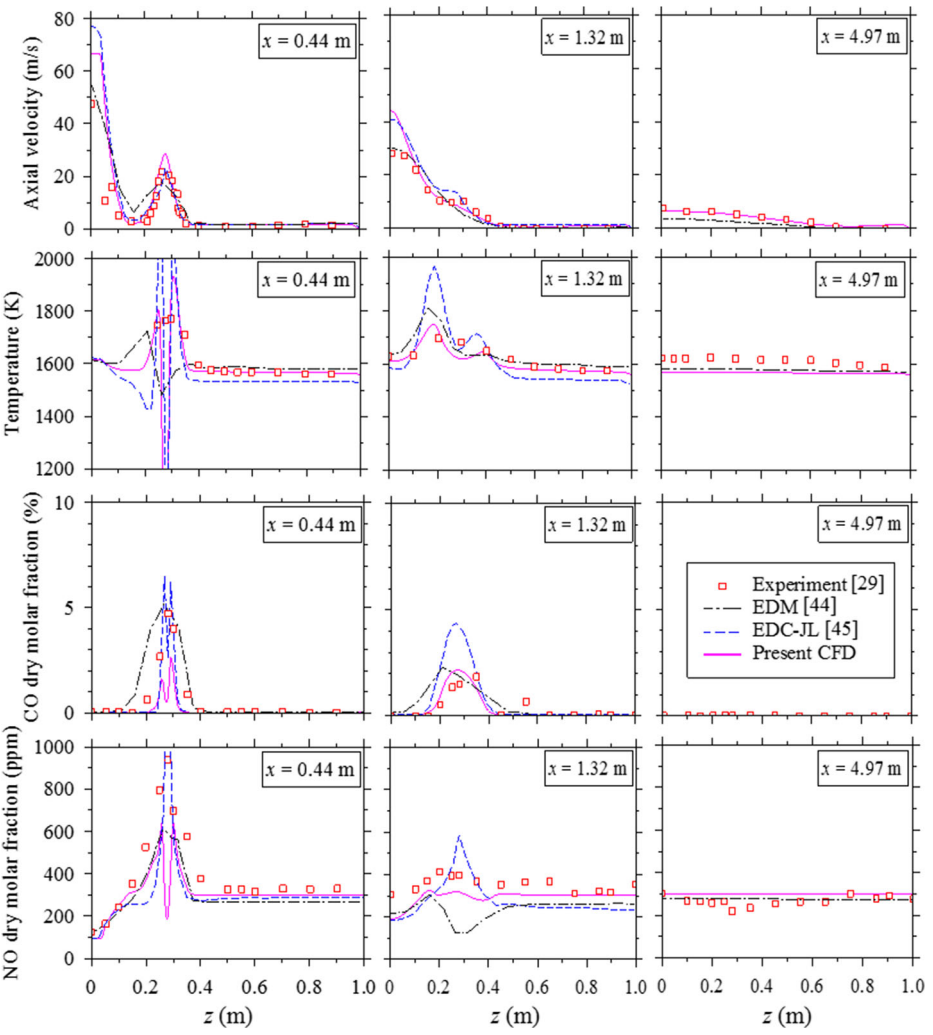

Fig. 2 Distributions of the numerical and experimental velocity, temperature, CO and NO molar fractions at $x = 0.44$, 1.32 and 4.97 m

that, in the IFRF experiment of coal combustion, the central air jet was not seeded, and only a small amount of coal particles was entrained by the central air jet in the downstream region near the central nozzle. These resulted in a poor signal in the LDA measurements in that region.

At the traverse of $x = 0.44$ m, all the predicted temperatures, CO and NO concentrations of Vascellari et al. [45] and those of the present modeling are more or less distinct from the measurements of Weber et al. [29] The present calculated maximal temperature is about 1930 K, which is between the prediction of Schaffel et al. [44] ($\approx$ 1720 K) and that of Vascellari et al. [45] (>2000 K), while the experimental value [29] is about 1800 K. This mainly attributes to the difficulty for the simulations to predict the correct ignition position of the pulverized coal as in the experiment. Apparently, the modeling of Schaffel et al. [44] performs better on the ignition than the present modeling and that of Vascellari et al. [45] In

particular, the CO prediction of Schaffel et al. [44] agrees very well with the measurement. The authors themselves however regarded the good agreement as coincidental because they employed the simplified two-step reaction mechanism for the volatile oxidation and the simplest one-reaction kinetic mechanism for the char oxidation. The reaction rates predicted by their simplified kinetic mechanisms are generally higher than those by multi-step kinetic mechanisms which are used in the present and Vascellari et al.'s simulations [45], so that the ignition delay is compensated in the former case. Nevertheless, in the downstream area at $x \geq 0.735$ m of the ignition region, the present predicted CO distributions agree well with the measurements.

Figure 2 also shows that the experimental NO profiles at $x = 0.44$ and 1.32 m cannot be well predicted by the present simulation and those of Schaffel et al. [44] and Vascellari et al. [45]. More specifically, at $x = 0.44$ m, the peak in NO distribution from Vascellari et al. [45] is approximately 2000 ppm compared to the experimental value of about 950 ppm; while those from the present and Schaffel et al. [44] are about 650 ppm. This is because, in the post processing approach, the transport equations of NO are solved based on the given flow field, temperatures and major combustion product concentrations. An accurate combustion solution is a necessary prerequisite to the accurate prediction of NO. Moreover, since the calculated temperature and CO concentration at $x = 0.44$ m are not perfect, the predicted NO profile cannot be very satisfactory. Nevertheless, no substantial difference of the NO distributions between the calculations and the measurements is seen at the traverse of $x = 4.97$ m. Hence, the predicted NO concentration in the downstream region should be considered more reliable than that at $x < 4.97$ m.

Here worth noting is that the NO formation rates in the present modeling, as well as Schaffel et al. [44], are obtained from different routes (i.e., thermal-NO, prompt-NO, fuel-NO, N_2O-NO and NO-reburning). Table 5 compares the detailed results from the two simulations. It is seen that the present maximal NO rates are generally higher than those of Schaffel et al. [44] by up to one order of magnitude. From the NO kinetic mechanisms (Eqs. 1 – 26), the distinctions are likely attributed to different temperatures and O_2 concentrations obtained by the present simulation and that of Schaffel et al. [44]. This suggests that the predicted in-furnace distributions of the thermal-NO, prompt-NO, fuel-NO, N_2O-NO and NO-reburning can be used only for the qualitative analysis. On the other hand, the present integrations of the fuel-NO rate and the NO-reburning rate over the entire furnace are nearly identical to those obtained by Schaffel et al. [44] Plus, as expected, both simulations predict that the fuel-NO formation rate and the NO-reburning rate are much

Table 5 NO formation rates via different routes obtained presently and by Schaffel et al. [44]

Route	Schaffel et al. [44]		Present	
	NO varying range [kmol/(m^{3}s)]	Integration over the entire furnace [kg/s]	NO varying range [kmol/(m^{3}s)]	Integration over the entire furnace [kg/s]
Thermal-NO	$0 \sim 6.6 \times 10^{-8}$	–	$0 \sim 8.9 \times 10^{-7}$	–
Prompt-NO	$0 \sim 1.6 \times 10^{-6}$	–	$0 \sim 7.4 \times 10^{-6}$	–
Fuel-NO	$-2.7 \times 10^{-4} \sim 7.8 \times 10^{-4}$	18.5×10^{-6}	$-1.0 \sim 3.3 \times 10^{-3}$	18.3×10^{-6}
N_2O-NO	$-2.0 \times 10^{-4} \sim 4.6 \times 10^{-9}$	–	$0 \sim 3.1 \times 10^{-8}$	–
NO-reburning	$-2.7 \times 10^{-4} \sim 0$	-11.5×10^{-6}	$0 \sim -1.5 \times 10^{-3}$	-11.7×10^{-6}

higher than those of thermal-NO, prompt-NO and N_2O-NO. As a result, the exhaust NO emission is correctly predicted by both simulations. Table 6 shows the value of 322 ppm from the present simulation and 333 ppm from Schaffel et al. [44] when comparing with the measured value of 320 ppm [29]. In addition, the calculated and measured parameters of the exhaust gas at the furnace exit are also compared in Table 6. Obviously, apart from the NO emission, the calculated temperature, O2, CO2, and CO concentrations are all comparable to the measurements. Of note, also, the measured CO emission at the furnace exit is less than 50 ppm (dry molar fraction), which indicates that pulverized coal combustion was well burnt out in the experiment. Overall, the present simulation predicts satisfactorily both in the furnace and at the furnace exit and so did those of Schaffel et al. [44] and Vascellari et al. [45].

It is important to note that Schaffel et al. [44] employed the simplified two-step reaction mechanism of the volatile oxidation, the simplest one-reaction kinetic mechanism of the char oxidation ($C_{(s)} + 0.5O_2 \rightarrow CO$) and the EDM, while Vascellari et al. [45] used the Multi-Step Combustion Mechanism for the volatile, oxidation and gasification kinetic mechanisms of the char ($C_{(s)} + 0.5O_2 \rightarrow CO$, $C_{(s)} + CO_2 \rightarrow 2CO$, $C_{(s)} + H_2O \rightarrow CO + H_2$) and the EDC model. Considering high CO_2, H_2O and low O_2 concentrations in the coal MILD combustion, the kinetics modeling of Vascellari et al. [45] is preferred in the present simulation for all the cases.

3.2 Effect of the fuel injection angle (α)

The simulations for $\alpha = -10^\circ \sim +15^\circ$ (Cases $1 \sim 6$) were made with $S = 0.28$ m and other operating parameters given in Table 3, which are identical to those of Weber et al. [29] The negative value of α indicates that the primary air-carrying-fuel jets are injected towards the central secondary air jet while the positive value indicates that the primary jets are injected deviated from the secondary jet.

Figure 3 shows the velocity distributions in the x-z plane for $\alpha = -10^\circ \sim +15^\circ$. The primary air jets carrying the pulverized coal are injected into the furnace via the side pipes, which are separated from the central secondary air jet. Both of the primary and secondary jets entrain and mix with the surrounding hot near-zero oxygen flue gases and become more diluted as they proceed downstream. For Cases $1 \sim 6$, when α is increased from -10° to $+15^\circ$, the confluence location of the primary and secondary jets moves significantly farther downstream from the injection nozzles. This implies that the oxygen concentration is diluted to lower levels in larger α case. That is, varying α strongly affects the temperature and reactions in the confluence region. Note that the mass flow rate of the primary air is much less than that of the secondary air and the pulverized coal is far from burning out with the primary air before the supply of oxygen from the secondary air.

Table 6 Present predictions and previous measurements [29] of exhaust gases at the furnace exit

	Unit	Experiment [29]	Calculation of Schaffel et al. [44]	Present calculation
Temperature	K	1503	1555	1523
O_2	vol. % dry	3.17	2.52	2.79
CO_2	vol. % dry	25.49	23.93	23.81
CO	vol. ppm dry	<50	10	33.78
NO	vol. ppm dry	320	333	322

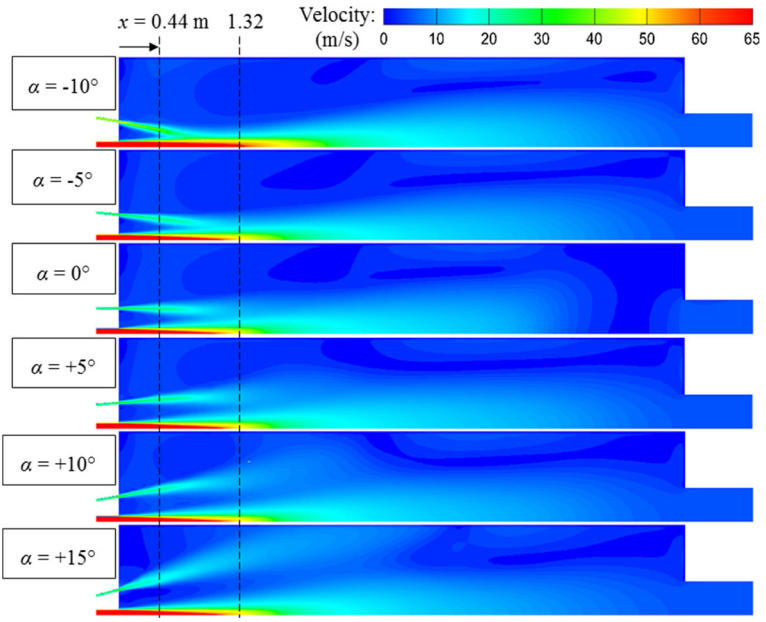

Fig. 3 Velocity distributions in the x-z plane for Cases 1$\sim$ 6

Figure 4 shows lateral profiles of the axial velocity component and the mean temperature at $x = 1.32$ m and 2.05 m for Cases 3$\sim$ 6 with $\alpha = 0° \sim +15°$. As demonstrated, when $x = 1.32$ m, the velocity hump appears over $z = 0.23 \sim 0.60$ m for $\alpha = +5°$ and $0.27 \sim 0.70$ for $\alpha = +10°$ and is nearer to the side walls for $\alpha = +15°$. Correspondingly, the temperature profile peaks doubly at $z = 0.23$ & 0.50 ($\alpha = +5°$), 0.27 & 0.67 ($\alpha = +10°$), and 0.43 & 0.83 ($\alpha = +15°$). (Note that the velocity hump means the central primary jet whereas the temperature peak reflects the center of the reaction zone in the jet mixing region.) Downstream to $x = 2.05$ m, the velocity profile becomes nearly flat for $\alpha = +5°$ and $+10°$, but for $\alpha = +15°$ the velocity hump is still apparent and close to the side walls, which is more clearly demonstrated by the temperature peak. These indicates that for $\alpha = +5° \sim +10°$, the primary air is sufficiently away from the side walls even at $x = 2.05$ m and the primary jets do not impinge the furnace walls. Differently, however, for the case of $\alpha = +15°$, the primary air jets appear to hit the walls while the combustion zones at the traverse location $x = 2.05$ m are very close to the side walls. This is likely to result in hot coal particles impinging and sticking to the side walls, so that the furnace may be damaged. Hence, excessively large injection angle of the primary air stream should be avoided in the industrial applications.

Figure 5 shows the temperature distributions in the x–z plane for $\alpha = -10° \sim +15°$. This plot reveals that there are relatively two high temperature zones for $\alpha = -10° \sim +10°$, which are located in the ignition region (IR) and the confluence region (CR) of the primary and secondary jets. Obviously, as α is increased from $-10°$ to $+10°$, the temperature distribution becomes more uniform; the IR peak temperature (T_{IR}) varies insignificantly by less than 30 K; and the CR peak temperature (T_{CR}) decreases significantly by 254 K (i.e., from 1923 K to 1669 K) whereas its x-location increases.

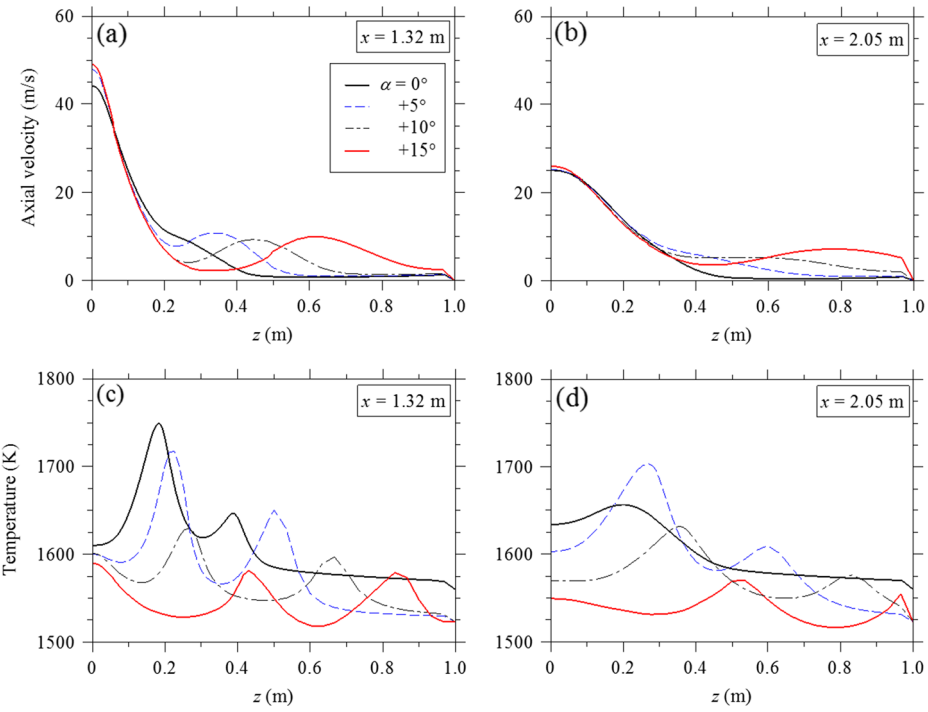

Fig. 4 Axial velocity profiles at two traverses of $x = 1.32$ and 2.05 m for Cases 3 ∼ 6

To explain this, the recirculation rate (K_v), which significant affects the performance of MILD combustion [2], is employed to investigate the oxygen dilution level in different cases. In the present CFD modeling, K_v is calculated as $K_v = m_r / (m_f + m_{pri} + m_{sec})$, where m_r is the mass flow rate of the entrained flue gas, m_f is the coal mass flow rate and $m_{pri} + m_{sec}$ denotes the total mass flow rate of the primary and secondary air streams. According to the mass conservation law, at each cross-section of the chamber, the mass flow rate of the flue gas entrained (m_r) by the fuel and oxidant jets must be equal to that of the recirculated gas downstream. The recirculated gas downstream can be well identified by the negative value of the local x-velocity. Thus, m_r at different x is calculated by

$$m_r(x) = \iint_{A(x)} \rho v_x(y, z) d\, y\, d \tag{27}$$

where $A(x)$ is the area for $v_x(y, z) < 0$.

Figure 6 shows the values of K_v for $x = 0.44$ m, 1.32 m and the x-location of T_{CR} for Cases 1 ∼ 5. The $x-$location of T_{IR} in the ignition region is close to $x = 0.44$ m, thus K_v at $x = 0.44$ m is regarded as the indication of the oxygen dilution level in the IR. The value of K_v at the x-location of T_{CR}, denoted by x_{TCR}, reflects the oxygen dilution level in the CR. Obviously, from Fig. 6, when $\alpha$is increased from $-10°$ to $+10°$, K_v increases slightly by less than 3.5 % at $x = 0.44$ m, while K_v increases significantly by 90.9 % at x_{TCR}. That is, increasing α only slightly affects the oxygen dilution level in the IR, hence T_{IR}, but strongly dilutes the reactants in the CR and thus decreases T_{CR}. It follows that the use of positive angles should achieve more stable MILD combustion than the $\alpha = 0°$ case.

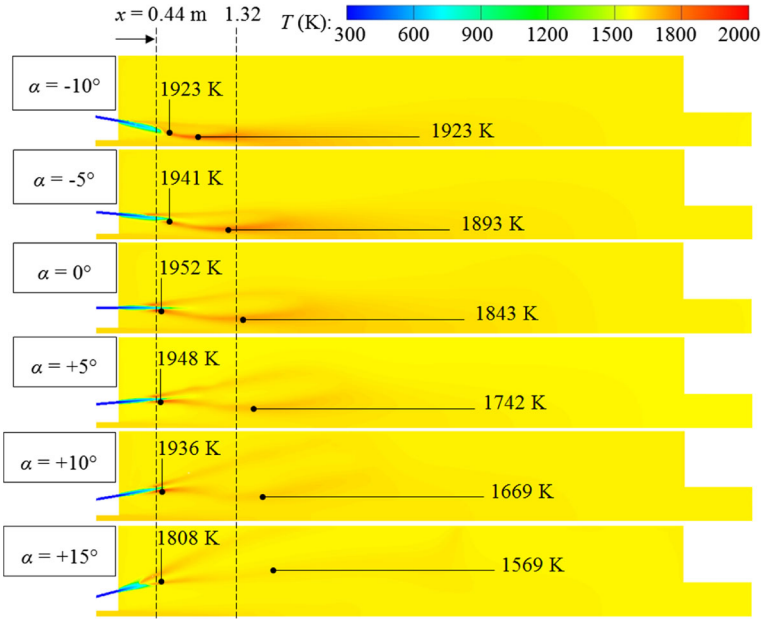

Fig. 5 Temperature distributions in the x-z plane for Cases 1 ∼ 6

This deduction is based on the above and the experimental observation of Wünning et al. [2] They found that, when sufficiently high furnace temperature (T_{furn} >fuel ignition temperature) and exhaust gas recirculation rate (K_v >2.5) are obtained, e.g., T_{furn} >1300K & K_v >3, the stable MILD combustion of natural gas can be well achieved. Indeed, the stable MILD combustion of firing pulverized-coal was achieved in the IFRF experiment [29] (i.e., the case of $\alpha = 0°$), with the secondary air being highly preheated to 1623 K. Assuming that the similar is obtained by the present simulation for $\alpha = 0°$, more stable MILD

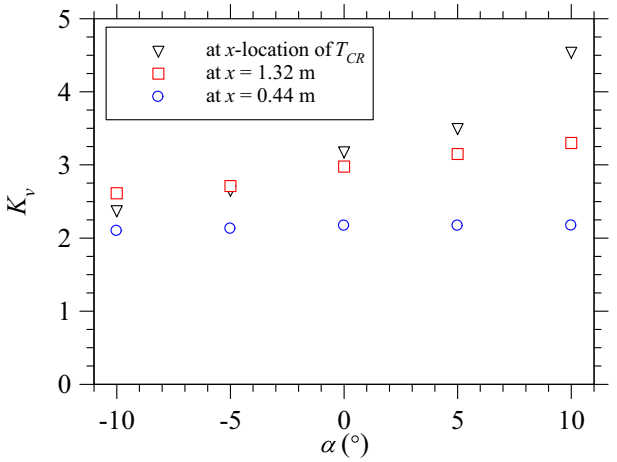

Fig. 6 Recirculation rate (K_v) at $x = 0.44$ m, 1.32 m and the x-location of T_{CR} for Cases 1 ∼ 5

combustion must be achieved for cases of $\alpha > 0°$, where both more uniform temperature distributions (Figs. 4 and 5) and higher recirculation rates (Fig. 6) occur. Besides, the furnace temperatures for the cases of $\alpha = 0° \sim +10°$ are all beyond 1500 K (surely >the ignition temperature).

Figure 7 shows the NO emissions via thermal, prompt, intermediate-N_2O, fuel and reburning routes at the furnace exit for $\alpha = -10° \sim +10°$. Although, for the experimental validation (Section 3.1), the simulation for the case of $\alpha = 0°$ uses the polluted secondary air with NO at 89 ppm, those for the effects of $\alpha$and S, whose results are displayed in Figs. 7, 13 and 17, employ the non-polluted air. Here it should be noted that the exhaust NO emissions obtained from the polluted and non-polluted treatments differ as expected, with 322 ppm for the former and 240 ppm for the latter.

Figure 7 demonstrates that, relative to the total NO emissions, the NO emissions from the thermal, prompt and intermediate-N_2O routes are negligible (totally <5 ppm), and their summed contribution accounts for less than 2 % of the total. This can be explained. In Cases 1 ∼ 5, all the temperature peaks are less than 1952 K. Due to the high activation temperature of Reaction 1 ($O + N_2 \Leftrightarrow N + NO$), the thermal NO generation rate is very low when the temperature is less than 2150 K, see Ref. [63]. For the intermediate-N_2O route, N_2 and O can react with each other over a low-temperature range because Reaction 17 ($N_2 + O + M \Leftrightarrow N_2O + M$) involves a third body M, thus the intermediate-N_2O route plays an important role in the production of NO under low-temperature and fuel-lean conditions [40], and dominates the total NO emission when the temperature <1300 K [21]. However, in the present simulations, the mean temperature in the furnace is beyond 1540 K, thus the NO emission via the intermediate-N_2O route is very low and can be ignored. For the prompt NO, it is formed in the fuel-rich condition, and the rate limiting step is Reaction 7 ($CH + N_2 \Leftrightarrow HCN + N$). In the present cases, the CH_x concentration relies on the devolatilization rate of volatiles from the pulverized coal, and the strong entrainments of the flue gases make the CH_x concentration diluted to low levels. From Fig. 7, obviously, the NO emission is mainly formed through the fuel-NO route. It is known that when the temperature is less than 2200 K,

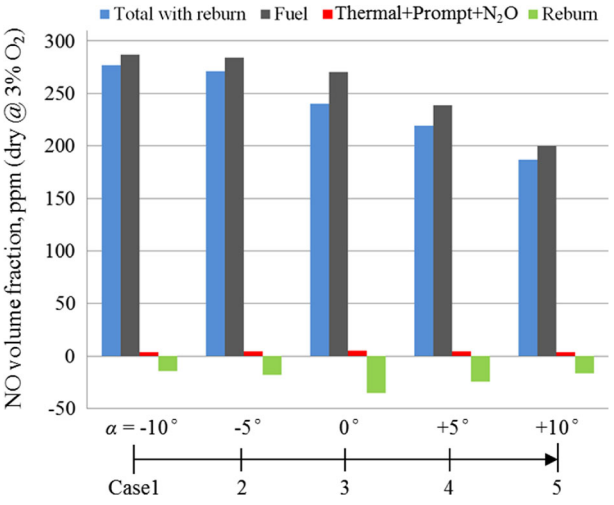

Fig. 7 NO emissions via thermal, prompt, intermediate-N_2O, fuel and reburning routes at the furnace exit for Cases 1 ∼ 5

varying temperature has slight effects on the fuel-NO formation [63]. In Cases 1 $\sim$ 5 with $\alpha = -10^\circ \sim +10^\circ$, the temperature is less than 2000 K over the whole furnace. Increasing α from -10° to $+10^\circ$ leads to a stronger entrainment of the flue gases and then a lower O_2 concentration, thus making the fuel-NO to decrease significantly from 287 ppm to 191 ppm. Figure 7 also shows that the NO-reburning mechanism cannot be ignored for all the cases. When α is increased from -10° to 0°, the reduced NO emission by reburning increases from 14 ppm to 35 ppm. This mainly attributes to that when the primary air is injected towards the secondary air with $\alpha < 0^\circ$, their merging is realized quickly, thus the fuel-rich region produced by the separated air nozzles become small. When α is increased from 0° to 10°, the reduced NO emission by reburning decreases from 35 to 17 ppm. This is relevant to the stronger dilution of the flue gases and lower level of the total NO concentrations in larger α cases. As a consequence, the reduction of NO by reburning is enhanced when α is increased from -10° to 0°, and a further increase of α from 0° to $+10^\circ$ weakens the NO-reburning.

In MILD combustion of the pulverized coal, the peak temperature is significantly suppressed and the oxygen is strongly diluted by the flue gases, which benefit for low NO emissions. However, these two characteristics are not good for the ignition and burnout of the pulverized coal. Figure 8 shows the distribution of the char concentration for $\alpha = -10^\circ \sim +10^\circ$. Obviously, after the coal enters the furnace, the char quickly decreases in concentration and is almost completely oxidized or gasified before reaching $x = 2.1$ m. That is, although the fuel stream is injected at quite a large angle from the secondary air stream, the complete oxidization or gasification of the char can be easily obtained with low peak temperature and O_2 concentration. This is mainly due to the highly preheated secondary air, which makes the temperature remain higher than 1540 K over the whole furnace. Although the local O_2 level is relatively low in coal MILD combustion, the char can also react with the surrounding CO_2 and H_2O at that high temperature level, and convert to gaseous CO and H_2. That is, the char gasification compensates the effects of the low O_2 concentrations on the complete combustion of the pulverized coal. Indeed, in the experiment of

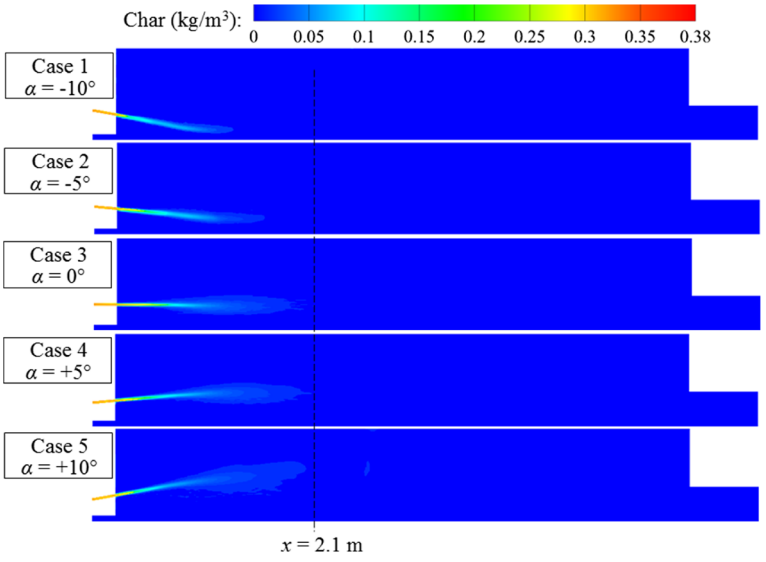

Fig. 8 Distributions of char concentrations (kg/m^3) in the x-z plane for Cases 1$\sim$5

Weber et al. [29], the coal MILD combustion is obtained with low NO emissions and also low CO emissions (<50 vol. ppm dry), see Table 6.

Here the CO emissions at the furnace exit for different injection angle (α) are examined. As demonstrated in Fig. 9, when $\alpha$is increased from $-10°$ to $+10°$, the temperature of the flue gases at the furnace exit slightly decreases from 1527 K to 1518 K. This is because for higher α, the high temperature region is located more closely to the furnace walls so that more heat may be transferred to the outside of the furnace through the walls (see Fig. 5). Figure 9 also shows that increasing α from $-10°$ to $+10°$ reduces the CO emission significantly from 128 to 12 ppm at the furnace exit. This is because more CO converts to CO_2 through the reversible reaction at lower temperatures. From Figs. 8 and 9, it is evident that the positive fuel injection angles still lead to complete combustion of the pulverized coal.

It is worth noting that the above results agree well with those previously obtained for the MILD combustion of firing gaseous fuels. Sobiesiak et al. [52] experimentally investigated the performance characteristics of the low-NO_x CGRI (Canadian Gas Research Institute) burner with high air preheat. The fuel injection angle was ranged from $+30°$ to $+65°$. By appropriate choice of the angle, ultralow NO_x emissions (2 ppm) were obtained and the combustion stability was enhanced. Similarly, for the CGRI burner with the fuel nozzle angle fixed at $+15°$, Fleck et al. [46] found that the combustion was visually flameless and very low NO_x emissions (6 ppm) were achieved. Besides, Li et al. [47] and Su et al. [48] numerically investigated the burners with positive fuel nozzle angles. As expected, the temperature peaks drop and the NO_x emissions decrease with the increasing of the fuel jet angels. These offers more evidence in support for the present observation.

3.3 Effects of the separation distance of the primary-secondary air nozzles (S)

The simulation results for Cases 7 $\sim$ 11 ($S = 0.10 \sim 0.60$ m and $\alpha = 0°$) are shown in Figs. 10–15. The velocity contours of Fig. 10 reveal that expectedly, as S is increased, the location of confluence between the primary and secondary streams shifts downstream. For $S = 0.10$ m, the primary and secondary air streams merge together immediately after issuing into the furnace. For $S = 0.28 \sim 0.60$ m, the primary air stream is clearly separated from the secondary air stream even at the traverse of $x = 0.44$ m.

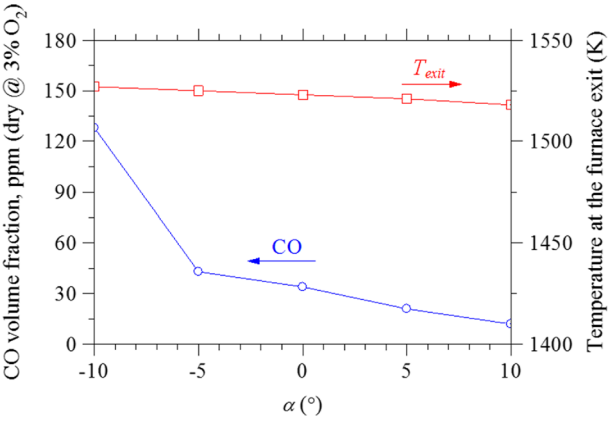

Fig. 9 CO emissions and temperatures at the furnace exit for Cases 1 $\sim$ 5

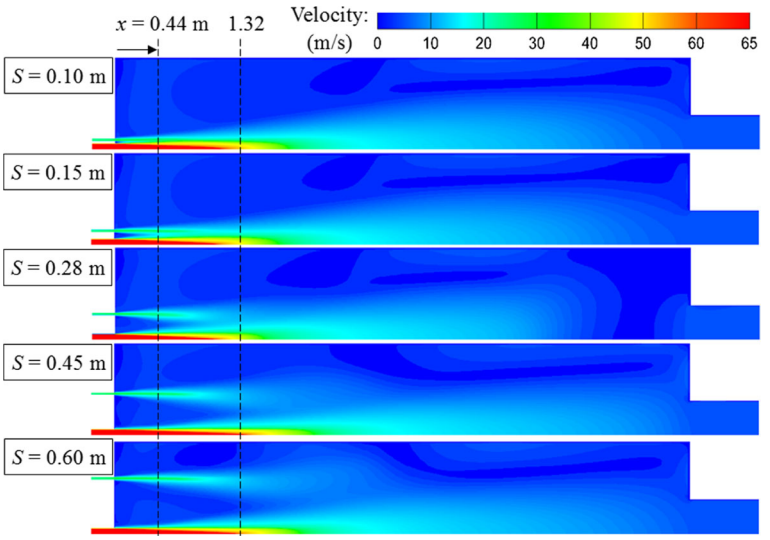

Fig. 10 Velocity distributions in the x-z plane for Cases 7 $\sim$ 11

Temperature contours in the x-z plane for Cases 7 $\sim$ 11 are displayed in Fig. 11. It is shown that the temperature distribution becomes more uniform when S is increased. T_{IR} remains almost the same when S is increased from 0.15 to 0.60 m, while a decrease of S from 0.15 to 0.10 m leads to a significant increase of T_{IR} (about 80 K). In contrast, T_{CR} decreases consistently from 2173 K to 1626 K when S is increased from 0.10 to 0.60 m. These observations are explained here. Figure 12 shows that decreasing S has only a slight effect on the recirculation rate of the flue gases over the whole domain, i.e., $K_v$is almost kept identical at $x = 0.44$ m when S is increased from 0.15 to 0.60 m. This is because, for

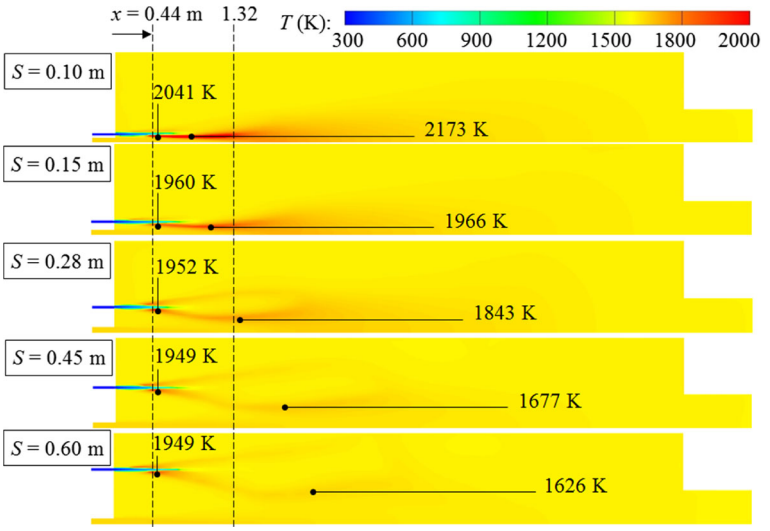

Fig. 11 Temperature distributions in the x-z plane for Cases 7 $\sim$ 11

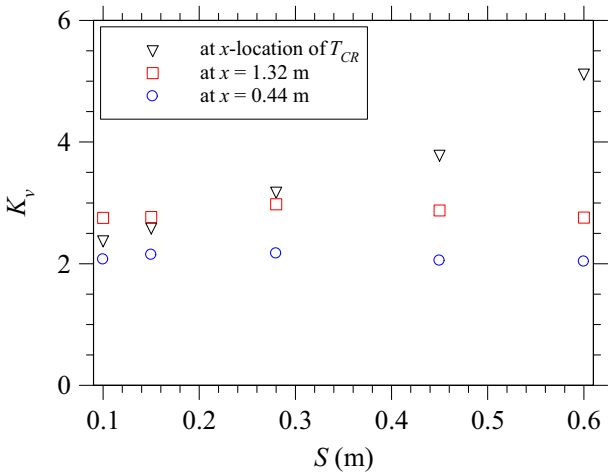

Fig. 12 Recirculation rate K_v at the traverses of $x = 0.44$ m, 1.32 m and the x-location of T_{CR} for Cases $7 \sim 11$

$S = 0.15 \sim 0.60$ m, the primary fuel jet is not mixed with the secondary air jet at $x = 0.44$ m or even beyond and so the ignition zone or the related temperature depends on the primary jet and its mixing with the surrounding flue gas but very weakly on the secondary air. For $S = 0.10$ m, however, the separation distance of the nozzles is so small that the primary and secondary jets merge almost immediately, thus the O_2 level in the ignition zone is increased significantly. Besides, increasing S from 0.10 m to 0.60 m consistently makes the confluence location shift downstream dramatically, consequently K_v at the x-location of T_{CR} increasing by 114.8 % and thus T_{CR} decreasing by 547 K.

The NO emissions from thermal, prompt, intermediate-N_2O, fuel and reburning routes at the furnace exit for Cases $7 \sim 11$ are presented in Fig. 13. As expected, the NO emissions from the first three routes are negligible (<7 ppm) for $S = 0.15 \sim 0.60$ m while their total contribution is about 4.7 % for $S = 0.10$ m. This is attributed to the fact that, the peak temperature ≤ 1970 K for $S = 0.15 \sim 0.60$ m but ranges from 2040 to 2175 K for $S = 0.10$ m (see Fig. 11). Evidently, the fuel-NO production is the dominant contribution to the total NO_x emission for all the cases. Particularly it is well beyond 300 ppm for $S = 0.10$ m, which should be avoided in the practical applications. As S is increased from 0.1 to 0.6 m, the fuel-NO production consistently decreases by about 150 ppm. It is interesting to note that the fuel-NO production is always higher than the total emission of NO_x due to the reduction of NO_x emission by reburning. Figure 13 also demonstrates that the reburning NO reduction grows with S increasing from 0.1 to 0.28 m and then turns to drop when S increases further. The first observation may result from the widening of S which delays the merging of primary and secondary streams and thus enlarges the fuel-rich region, consequently benefiting for stronger NO-reburning. The second agrees well with Stadler et al. [64] who investigated NO_x emissions in oxycoal combustion and found that the NO-reburning effect is less pronounced at lower NO_x levels.

Figure 14 shows contour distributions of char concentrations (kg/m^3) in the x-z plane for Cases $7 \sim 11$. As demonstrated, although the fuel stream is separated with the secondary air stream by the distance S (e.g., 0.6 m), the char appears to be completely oxidized or gasified before it reaches $x = 2.7$ m. The gasification is attributed to the char reactions

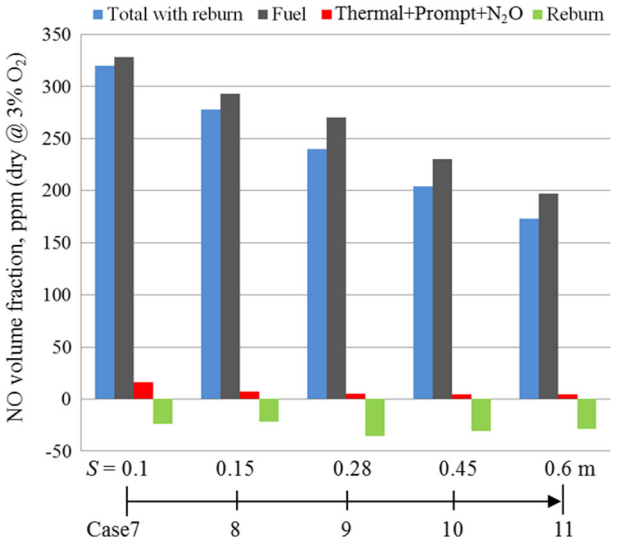

Fig. 13 NO emissions from thermal, prompt, intermediate-N_2O, fuel and reburning routes at the furnace exit for Cases 7 ∼ 11

with CO_2 and H_2O at high temperatures. Note that in the experiment of Weber et al. [29], the measured mass fraction of carbon in ash at the furnace exit is about 15 %, while the presently simulated char is completely combusted. Similar results were also observed in the simulations of Schaffel et al. [44] and Vascellari et al. [45] (i.e., 100 % char burnouts were obtained). This reflects that the char burnout is generally over predicted. As suggested by Schaffel et al. [44], corrections to the char model are needed to slow down the rate as the char oxidation proceeds. Nevertheless, the gasification of char with CO_2 and H_2O

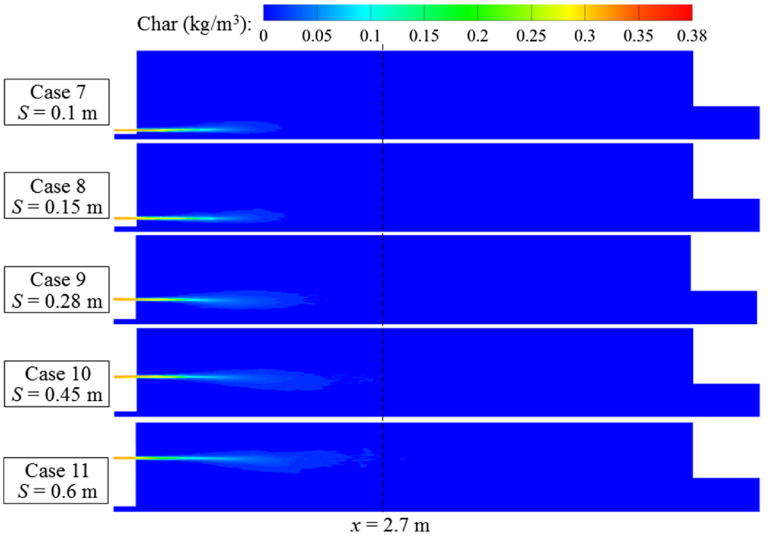

Fig. 14 Distributions of char concentrations (kg/m^3) in the x-z plane for Cases 7 ∼ 11

(i.e., C(s) $+CO_2 \rightarrow 2CO$, C(s) $+H_2O \rightarrow CO + H_2$) is very important in coal MILD combustion and should not be ignored in simulations.

Figure 15 shows the exhaust CO emissions and temperatures at the furnace exit for $S = 0.1 \sim 0.6$ m. As clearly seen, when S increases from 0.1 to 0.6 m, the CO emission significantly decreases from 104 to 4 ppm whereas the temperature reduces from 1530 to 1516 K. The first observation perhaps suggests that the widening separation of the primary and secondary nozzles is beneficial for the establishment of MILD combustion and achieves higher combustion efficiency. On the other hand, the second means that increasing S simultaneously results in less heat being carried out from the exit. Taking together, it appears to reflect that an increase in S enhances the heat transfer through the furnace wall to the outside. This can be sensibly explained here. In higher S cases, the high temperature region is closer to the furnace walls (see Fig. 11) and thus more heat is transfer to the outside of the furnace through the walls.

4 Further Discussions

In our previous work [25], the effects of diameters of the primary and secondary air nozzles (D_{pri} and D_{sec}) on coal MILD combustion in the IFRF furnace [29] were numerically investigated. Thus, to provide more complete information for the optimization of burner configuration, the effects of α and S on NO emissions are analyzed below together with those of D_{pri} and D_{sec}.

Figure 16 is the schematic diagram of recirculation rate (K_v) and the fuel-jet penetration location (x_p) in IFRF furnace. For the IFRF experiment, the rates of the inlet mass flow and momentum of the central secondary air jet are about 5.2 and 13.0 times those of the primary jets, respectively. Accordingly, the central secondary air jet is much stronger than the side primary jets, causing the latter inclining to and eventually merging into the former. From the previous studies [19, 23], $K_v(x = x_p)$ is a key quantity for establishing MILD combustion. Enhancing the entrainment of the flue gases or delaying the confluence of the fuel and oxidant streams results in a higher value of $K_v(x = x_p)$, thus benefiting for better performance of MILD combustion.

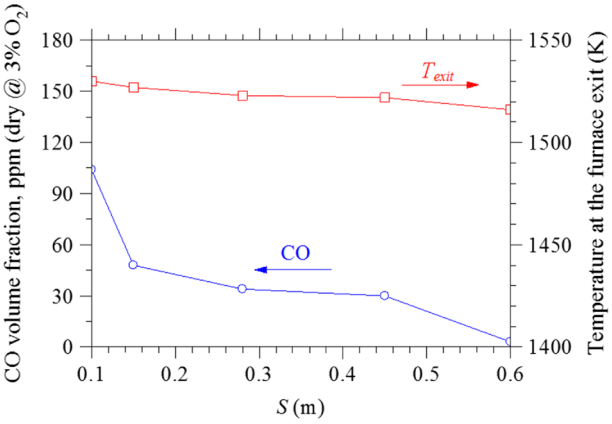

Fig. 15 CO emissions and temperatures at the furnace exit for Cases 7 ~ 11

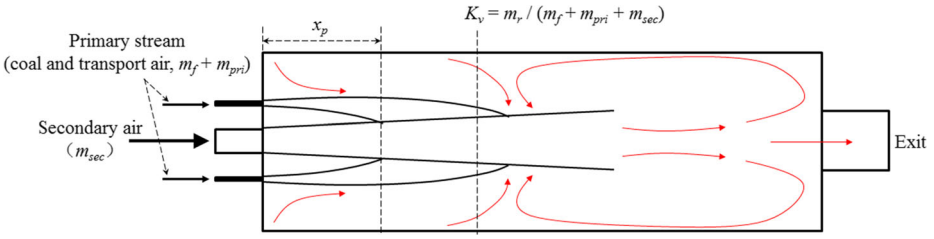

Fig. 16 Recirculation rate (K_v) and fuel-jet penetration location (x_p) in IFRF furnace

As shown in Ref. [25], since the mass flow rates of the primary and secondary air are kept constant, the velocities of the primary and secondary air (v^*_{pri} and v^*_{sec}) vary significantly with D_{pri} and D_{sec}. Although increasing v^*_{sec} (by decreasing D_{sec}) enhances the entrainment of flue gases, the confluence location of primary and secondary air streams simultaneously shifts upstream, which is a negative factor for establishing the coal MILD combustion. In contrast, a decrease in D_{pri} can significantly enhance the entrainment of the side jets and thus delay the confluence of the central and side jets, which is favorable for the occurrence of MILD condition. Likewise, an increase in α or S delays the confluence of the central and side jets, too. Figure 17 shows the NO emissions versus D_{pri}, D_{sec}, α and S. The injection momentum from the burner is calculated by the sum of the inlet momenta of the primary and secondary air jets. Apparently, decreasing D_{pri} for high primary jet speeds is the most effective way to obtain extremely low NO emissions (e.g., 41 ppm at 3 % O_2). However, the use of an excessively high velocity appears reversely to attain an unexpected high NO emission, perhaps due to the destruction of the fuel-rich and fuel-lean combustion configurations necessary for MILD condition. Figure 17 also shows that a decrease in D_{sec} virtually has no effect on the NO emission, thus an appropriately large D_{sec} is suggested for energy saving in air supply in industrial applications. In addition, it is worth noting that, when α or S is increased at a constant value of the injection momentum from the burner,

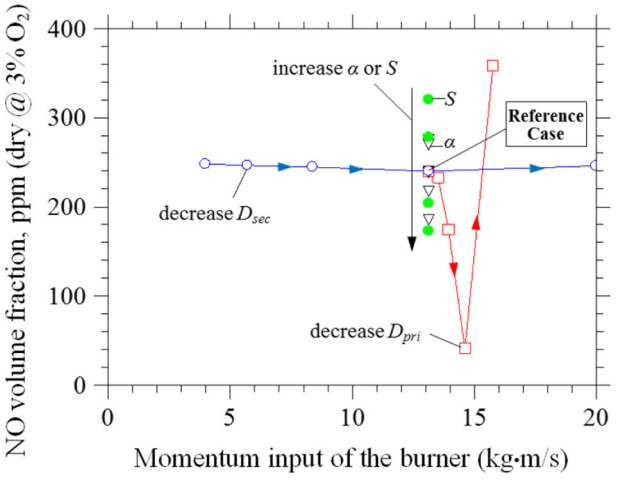

Fig. 17 NO emissions versus D_{pri}, D_{sec}, α and S of straight-flow burner in IFRF furnace

the NO emissions decrease significantly. That is, the increase of α or S is an effective way to suppress the NO emissions with no need for extra energy cost.

5 Conclusions

The present study has numerically investigated the effects of the fuel injection angle (α) and the separation distance of the primary-secondary air nozzles (S) on the MILD combustion of the pulverized coal. Based on the results shown in Sections 3 $\sim$ 4, several conclusions can be drawn below:

(1) Increasing α has a slight effect on the peak temperature in the ignition region but significantly reduces the peak temperature in the confluence region of the primary and secondary air streams, thus resulting in the decreased NO emission.
(2) Increasing S has only a minor effect on the recirculation rate of the flue gases over the whole domain but significantly shifts the confluence region downstream. Consequently, when S is increased from 0.1 to 0.6 m in the present case, the peak temperature in the confluence region decreases by 547 K and the NO emission at the furnace exit also decreases by 147 ppm.
(3) In coal MILD combustion, almost all the NO emission is formed through the fuel-NO route and the thermal, prompt and intermediate-N_2O routes contribute little. The NO-reburning mechanism is important that always reduces the NO emission. Nevertheless, the NO-reburning cannot be affected consistently by increasing αor S.
(4) In coal MILD combustion, the strong entrainment of flue gases significantly reduces the O_2 concentration but increases the concentrations of CO_2 and H_2O. Thus the gasification of char with CO_2 and H_2O (i.e., $C_{(s)} + CO_2 \rightarrow 2CO$ and $C_{(s)} + H_2O \rightarrow CO + H_2$) compensate the reduced rate of combustion reaction of the pulverized coal due to the low-oxygen fraction.
(5) To achieve a good design of coal MILD burner, it is essential to consider how to enhance the in-furnace recirculation rate of the flue gases and how to delay the confluence of the primary and secondary air streams. According to our present and previous work [28], decreasing D_{pri} is the most potential way to obtain extremely low NO emissions at an acceptable cost of extra electricity while increasing α or S is an effective way to suppress the NO emissions without consumption of any extra energy.

Acknowledgments The authors gratefully acknowledge the support of the Special Research Fund for the Doctoral Program of Higher Education of China (Grant No. 20110001130014), the Natural Science Foundation of China (Grant No. 51276002 and 51406001) and the China Postdoctoral Science Foundation (2014M550011).

References

1. Wünning, J.: Chemie Ingenieur Technik **63**(12), 1243–1245 (1991)
2. Wünning, J.A., Wünning, J.G.: Prog. Energy. Combust. Sci. **23**(1), 81–94 (1997)
3. Weber, R., Lverlaan, A., Orsino, S., Lallemant, N.: J. Inst. Energy **72**, 77-83 (1999)
4. Weber, R., Orsino, S., Lallemant, N., Verlaan, A.: Proc. Combust. Inst. **28**(1), 1315–1321 (2000)
5. Katsuki, M., Hasegawa, T.: Proc. Combust. Inst. **27**(2), 3135–3146 (1998)
6. Tsuji, H., Gupta A., Hasegawa, T., et al. CRC Press, Florida (2003)
7. Yang, W., Blasiak, W.: Energy **30**(2-4), 385–398 (2005)
8. Blasiak, W., Yang, W., Narayanan, K., von Scheele, J.: J. Energy Inst. **80**(1), 3–11 (2007)

9. de Joannon, M., Cavaliere, A., Faravelli, T., Ranzi, E., Sabia, P., Tregrossi, A.: Proc. Combust. Inst. **30**(2), 2605–2612 (2005)
10. de Joannon, M., Matarazzo, A., Sabla, P., Cavaliere, A.: Proc. Combust. Inst. **31**(2), 3409–3416 (2007)
11. Veríssimo, A.S., Rocha, A.M.A., Costa, M.: Exp. Therm. Fluid Sci. **44**, 75–81 (2013)
12. Veríssimo, A.S., Rocha, A.M.A., Costa, M.: Fuel Process. Technol. **106**, 423–428 (2013)
13. Dally, B.B., Riesmeier, E., Peters, N.: Combust. Flame **137**(4), 418–431 (2004)
14. Dally, B.B., Karpetis, A.N., Barlow, R.S.: Proc. Combust. Inst. **29**(1), 1147–1154 (2002)
15. Arghode, V.K., Gupta, A.K., Bryden, K.M.: Appl. Energy **92**, 822–830 (2012)
16. Arghode, V.K., Gupta, A.K.: Int. J. Hydrogen Energy **36**(10), 6292–6302 (2011)
17. Kumar, S., Paul, P.J., Mukunda, H.S.: Proc. Combust. Inst. **29**(1), 1131–1137 (2002)
18. Reddy, M.V., Sawant, D., Trivedi, D., Kumar, S.: Proc. Combust. Inst. **34**(2), 3319–3326 (2013)
19. Mi, J., Wang, F., Li, P., Dally, B.B.: Energy Fuels **26**(1), 265–277 (2012)
20. Wang, F., Li, P., Mei, Z., Zhang, J., Mi, J.: Energy (2014). doi:10.1016/j.energy.2014.05.029
21. Li, P., Dally, B.B., Mi, J., Wang, F.: Combust. Flame **160**(5), 933–946 (2013)
22. Mi, J., Li, P., Dally, B.B., Craig, R.A.: Energy Fuels **23**(11), 5349–5356 (2009)
23. Mi, J., Li, P., Zheng, C. Energy **36**(11), 6583–6595 (2011)
24. Li, P., Wang, F., Tu, Y., Mei, Z., Zhang, J., Zheng, Y., Liu, H., Liu, Z., Mi, J., Zheng, C.E.: Energy Fuels **28**(2), 1524–1535 (2014)
25. Mei, Z., Li, P., Wang, F., Zhang, J., Mi, J.: Energy Fuels **28**(1), 369–384 (2013)
26. Galbiati, M.A., Cavigiolo, A., Effuggi, A., Gelosa, D., Rota, R.: Combust. Sci. Technol. **176**(7), 1035–1054 (2004)
27. Derudi, M., Rota, R.: Proc. Combust. Inst. **33**(2), 3325–3332 (2011)
28. Lallemant, N., Breussin, F., Weber, R., Ekman, T., Dugue, J., Samaniego, J.M., Charon, O., Van Den Hoogen, A.J., Van Der Bemt, J., Fujisaki, W., Imanari, T., Nakamura, T., Iino, K.J.: Energy Inst. **73**, 169–182 (2000)
29. Weber, R., Smart, J.P., Kamp, v.d.W.: Proc. Combust. Inst. **30**(2), 2623–2629 (2005)
30. Cavaliere, A., de Joannon, M.: Prog. Energy Combust. Sci. **30**(4), 329–366 (2004)
31. Szegö, G.G., Dally, B.B., Nathan, G.J.: Combust. Flame **156**(2), 429–438 (2009)
32. Gao, X., Duan, F., Lim, S., Yip, M.: Energy **59**, 559–569 (2013)
33. Lille, S., Blasiak, W., Jewartowski, M.: Energy **30**(2), 373–384 (2005)
34. Smart, J.P., Riley, G.S.: J. Energy Inst. **85**(3), 131–134 (2012)
35. Suda, T., Takafuji, M., Hirata, T., Yoshino, M., Sato, J.: Proc. Combust. Ins.t **29**(1), 503–509 (2002)
36. Zhang, H., Yue, G., Lu, J., Jia, Z., Mao, J., Fujimori, T., Suko, T., Kiga, T.: Proc. Combust. Inst. **31**(2), 2779–2785 (2007)
37. Ponzio, A., Senthoorselvan, S., Yang, W., Blasiak, W., Eriksson, O.: Fuel **87**(6), 974–987 (2008)
38. Rathnam, R.K., Elliott, L.K., Wall, T.F., Liu, Y., Moghtaderi, B.: Fuel Process Technol. **90**(6), 797–802 (2009)
39. Stadler, H., Ristic, D., Förster, M., Schuster, A., Kneer, R., Scheffknecht, G.: Proc. Combust. Inst. **32**(2), 3131–3138 (2009)
40. Turns, S.R. McGraw Hill Higher Education, New York (1996)
41. Stadler, H., Toporov, D., Förster, M., Kneer, R.: Combust. Flame **156**(9), 1755–1763 (2009)
42. Schaffel-Mancini, N., Mancini, M., Szlek, A., Weber, R.: Energy **7**(35), 2752–2760 (2010)
43. Shaddix, C.R., Molina, A.: Proc. Combust. Inst. **33**(2), 1723–1730 (2011)
44. Schaffel, N., Mancini, M., Szlek, A., Weber, R.: Combust. Flame **156**(9), 1771–1784 (2009)
45. Vascellari, M., Cau, G.: Fuel **101**, 90–101 (2012)
46. Fleck, B.A., Sobiesiak, A., Becker, H.A.: Combust. Sci. Technol. **161**(1), 89–112 (2000)
47. Li, X., Wei, Z., Xu, L., Cheng Y.: Effect of inclined angle of fuel jet on NO_x emission in high temperature air combustion. International Conference on Imaging Systems and Techniques, 497–501 (2012)
48. Su, Y., Zhao, B.: CFD simulation of high temperature air combustion of coal gas at different air straddle angle. International Conference on Bioinformatics and Biomedical Engineering, 1–4 (2010)
49. Shih, T.H., Liou, W.W., Shabbir, A., Yang, Z., Zhu, J.: Comput. Fluids **24**(3), 227–238 (1995)
50. Gran, I., Magnussen, B.: Combust. Sci. Technol. **119**(1-6), 171–190 (1996)
51. Fletcher, T.H., Kerstein, A.R., Pugmire, R.J., Solum, M.S., Grant, D.M.: Energy Fuels **6**(4), 414–431 (1992)
52. Jones, W.P., Lindstedt, R.P.: Combust. Flame **73**(3), 233–249 (1988)
53. Cheng, P.: AIAA J. **2**(9), 1662–1664 (1964)
54. Zeldovich, Y.A., Frank-Kamenetskii, D., Sadovnikov, P.: Oxidation of nitrogen in combustion. Publishing House of the Acad of Sciences of USSR (1947)
55. Hanson, R.K., Salimian, S.: Survey of rate constants in the N/H/O system. Combustion chemistry, pp. 361–421. Springer, US (1984)

56. De Soete, G.G.: Proc. Combust. Inst. **15**(1), 1093–1102 (1975)
57. Smoot, L.D., Smith, P.J.: NO_x Pollutant formation in turbulent coal systems. Coal Combustion and Gasification, pp. 373–403. Springer, US (1985)
58. Melte, P.C., Pratt, D.T.: Proc. Combust. Inst. **15**(1), 1061–1070 (1975)
59. Kandamby, N., Lazopoulos, G., Lockwood, F.C., Perera, A., Vigevano, L.: Mathematical modeling of NO_x emission reduction by the use of reburn technology in utility boilers (1996)
60. Levy, J.M., Chen, L.K., Sarofim, A.F., Beer, J.M.: Proc. Combust. Inst. **18**(1), 111–120 (1981)
61. Abdel-Rahman, A.: WSEAS Trans Fluid Mechanics **4**(5), 257–275 (2010)
62. Orsino, S., Tamura, M., Stabat, P., Constantini, S., Prado, O., Weber, R.: Excess enthalpy combustion of coal. Technology Report IFRF Doc. No. f46/y/3, IFRF (2000)
63. Pershing, D.W., Wendt, J.O.L.: Proc. Combust. Inst. **16**(1), 389–399 (1977)
64. Stadler, H., Christ, D., Habermehl, M., Heil, P., Kellermann, A., Ohliger, A., Toporov, D., Kneer, R.: Fuel **90**(4), 1604–1611 (2011)